**IMAV2016-40**
http://www.imavs.org/pdf/imav.2016.40

# Tailless Control of a Double Clap-and-Fling Flapping Wing MAV

CHAN Woei Leong,* Nguyen Quoc Viet, and Marco DEBIASI
National University of Singapore

ABSTRACT

This paper presents the study on a tailless control mechanism designed to tilt the wing roots of a double clap-and-fling flapping wing micro-air-vehicle (MAV). The MAV has made stable hovering flight with tail and stabilizers, the work presented in this paper paves the way for the implementation of tailless flight control on the MAV. A wing tilting mechanism driven by three linear servos was designed and fabricated. Study shows that tilting the wing roots creates a linear trend of pitching and rolling moments if the centre of gravity (CG) falls on the correct location. Wing kinematics was captured and it was found that the higher drag due to higher angle of attack could be a contributing factor to the pitching and rolling moments. Another contributing factor could be the lift dissymmetry of the opposite pairs of wings. The effects of pitch-roll coupling are also presented.

## 1 INTRODUCTION

Tailless flapping wing is one of the most challenging aspects of flapping wing flight, mainly due to the complexity of the mechanism, the coupling effect of forces and moments that is yet to be fully understood, and the stability problem that arises once the tail is removed. Furthermore, there are quite a few types of flapping wings, including two-winged platforms that generate thrust or lift mainly by delayed stall and wake capture, four-winged platforms that utilize clap-and-fling, and tandem wing platforms that exploit the interactions of the forewings and hind wings. Implementing tailless control on each type of platform could be very different due to their differences in aerodynamics characteristics. However, despite the challenges, tailless control comes with the advantages of biomimicry, less sensitive to disturbance due to the absence of tail surfaces, and higher manoeuvrability.

The first step to achieve tailless control is to design a symmetrical gearbox. Such gearboxes ensure hovering equilibrium can be achieved. The Temasek Laboratories of the National University of Singapore has been developing flapping wing MAVs, including the Odopter [1] that encompasses a hybrid concept, and the FolowerFly [2] that is designed to hover and utilizes a symmetrical flapping mechanism. Our previous efforts on tailless control were focused on bench testing of two-winged platforms [3, 4]. Although the outcome was satisfactory, two-winged platforms tend to suffer from severe vibration and the lift generation is not as efficient as a four-winged clap-and-fling platform. Hence the decision to implement tailless control on the FlowerFly was made.

Similar effort has been done by different research groups, including Karasek et al. [5, 6], Takagi et al. [7], and Phan et al. [8]. The mechanisms used are mainly Type 1: changing the stroke angle and flapping rate to create lift and drag dissymmetry, which is harder to implement, or Type 2: manipulating the trailing edge of the wing roots, similar to the mechanism discussed in this paper. All of these efforts focus on two-winged platforms.

Some successful tailless flapping wing platforms include the Nano Hummingbird [9], FESTO BionicOpter [10], FESTO eMotionButterflies [11], and the Robobee [12, 13]. Among these platforms, the Nano Hummingbird which utilizes the aforementioned Type 2 mechanism, stands out as the most impressive standalone platform. Although the Robobee which utilizes Type 1 mechanism is a tethered platform, it is the most outstanding in terms of fabrication techniques and miniturization.

This paper focuses on the implementation of a Type 2 tailless control mechanism and its implementation on a four-winged clap-and-fling flapping wing platform. Section II of this paper elaborates the flapping mechanism, the wing, and the wing tilt mechanism. The experiment setup is being explained in Section III. The experiment results are presented and discussed in Section IV. Finally, the concluding remarks end the paper.

## 2 FLAPPING MECHANISM, WING, AND WING TILT MECHANISM

### *2.1 Flapping Mechanism*

The flapping mechanism of the FlowerFly MAV [2] is used in this study. It is a four-winged flapping mechanism which utilizes double clap-and-fling. The wings clap at the front and rear at the end of down stroke and clap at the right and left at the end of upstroke. This unique design fully utilizes the whole volume around the MAVs body, maximizing the wing swept volume for lift generation. It is designed to be symmetrical such that the net lift acted at the centre of the flapping mechanism, allowing the MAV to hover at equilibrium with tail attached.

*Email address(es): tslcwl@nus.edu.sg



IMAV 2016, Beijing, PR of China, 17-21 October 2016
International Micro Air Vehicle Competition and Conference 2016

### 2.2 *Wing*

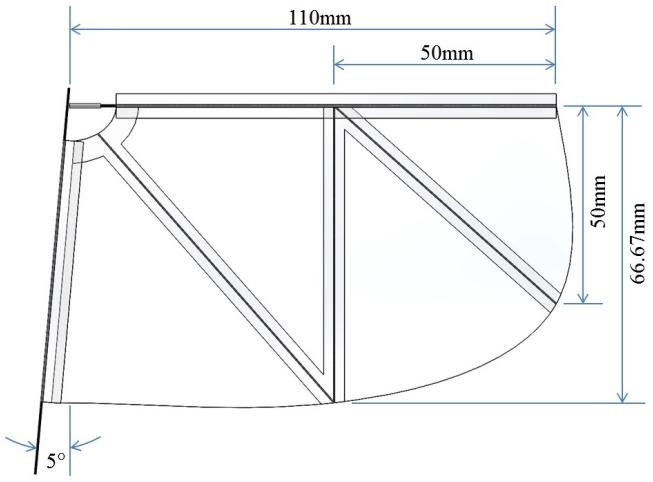


Figure 1: Wing dimension.

The wing has a root-to-tip wingspan of 110mm and the maximum chord length of 66.67mm. At the wing root, there is a $5^\circ$ of slack angle to encourage wing rotation.

The wing membrane is $10\mu$m Mylar film. The leading edge, wing root, and stiffeners are carbon rods at diameter of 0.6mm, 0.5mm, and 0.25mm respectively. The carbon rods are attached on the wing membrane with $23.4\mu$m transparent polyester stickers. The total weight of one wing is 0.29g.

### 2.3 *Wing Tilt Mechanism*

The wing tilt mechanism is driven by three linear servos. Two servos are attached on the body right under the flapping mechanism, and one attached at the bottom of the body as shown in Figure 2. Servo 1 and 2 are used to push and pull the pitching arms. The pitching arms are attached on the rolling arm, which is driven by Servo 3. The wing roots are attached to the pitching arms such that the wings can be tilted longitudinally (forward and rearward) using the pitching arms, and laterally (rightward and leftward) using the rolling arm.

The arms and the linkages are mainly CNC milled out of Delrin plastic, but the arms of Servo 1 and 2 are connected to the mechanism through ball links to minimize the coupling between pitch and roll. Due to limitation on space, the mechanism can tilt the wing roots within limited range of $\pm 2^\circ$ for both pitch and roll inputs.

### 2.4 *Coordinate System and Sign Convention*

The average tilting angle of the wing roots at longitudinal and lateral directions are given the designation of $\delta_p$ and $\delta_r$ respectively, which stand for pitch input and roll input. At neutral position, $\delta_p$ and $\delta_r$ are both zeros. In this study, tilting the wing root rearward and rightward are positive.

The coordinate system used is consistent with body-fixed coordinate system of aircraft flight dynamics: the origin at the centre of gravity, positive X, Y and Z directions coincide with

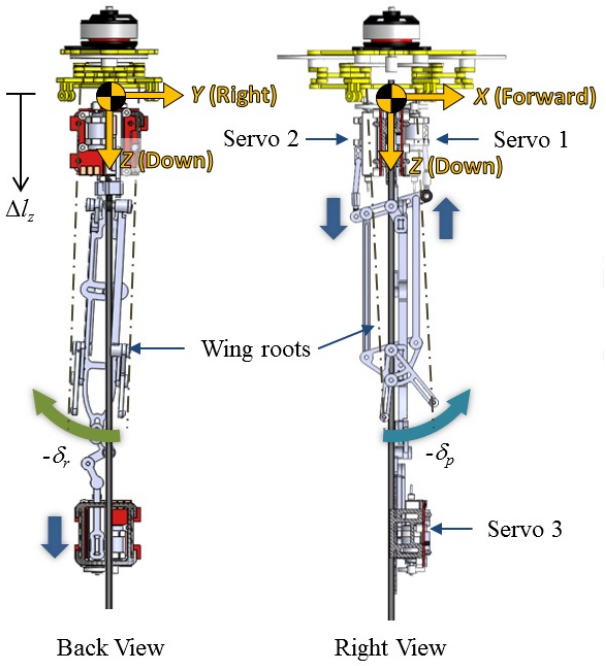


Figure 2: Wing tilt mechanism and coordinate system.

forward, rightward, and downward respectively as shown in Figure 2. The centre of gravity is assumed to be at the centre of the stroke plane. The force and moment data presented in this paper were transformed to this coordinate system, except for Section 4.3 where the assumed CG is shifted at $\Delta l_z$ to evaluate the effect of CG shift.

## 3 Experimental Setup

### 3.1 *Force and Moment Measurement*

Unlike our previous studies on two-winged platforms [3, 4], the four-winged platform produces less moment fluctuations, allowing a smaller load cell to be used for force and moment measurement at higher resolution. The flapping wing platform is attached on an ATI Nano17 Titanium as shown in Figure 3. The sampling rate used was 5000Hz.

Shunt resistors were used for current measurement. The power was supplied to the system through two 31 AWG enamelled wires as shown in Figure 4. The wires are at the right thickness to make sure the force and moment measurements, and the power supplied to the system are not compromised. The flapping frequency and wing tilt angles were controlled using a remote control radio. The flapping frequency was measured using a magnet attached on the main gear and a Hall Effect switch. The same signal from the Hall Effect switch was used as trigger signal for load cell and high speed camera.

### 3.2 *Wing Kinematics Capture*

The wing kinematics of the front left wing was captured using similar technique in our previous studies [4].

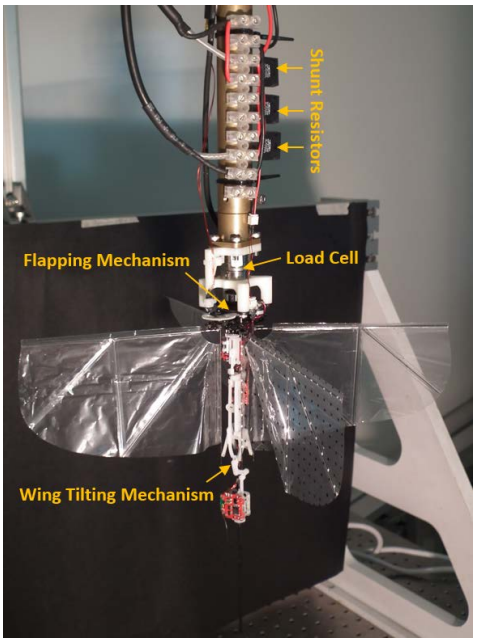


Figure 3: Experimental setup for force and moment measurement.

High speed videos of the flapping wings with markers were recorded using the Phantom Miro 320S high speed camera at 5000Hz from three different viewing angles. Using one camera, the three viewing angles were achieved by fixing the camera at one position, and rotate the flapping wing platform. The trigger signal ensures the video recording always starts at the same wing position. The wing kinematics repeatability was satisfactory. Figure 5 shows the snapshots of high speed video from three viewing angles. Theoretically, two viewing angles are enough to reconstruct the wing kinematics, but three viewing angles reduces the blind spots significantly. The wing kinematics was reconstructed using the open source Matlab code from Hedrick [14].

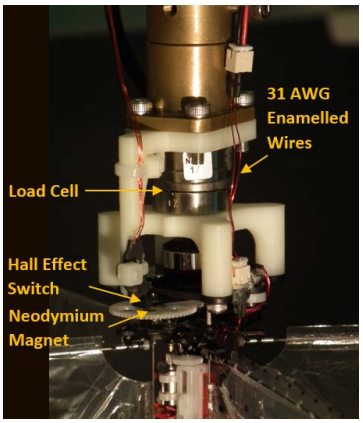


Figure 4: Close-up view of the experimental setup.

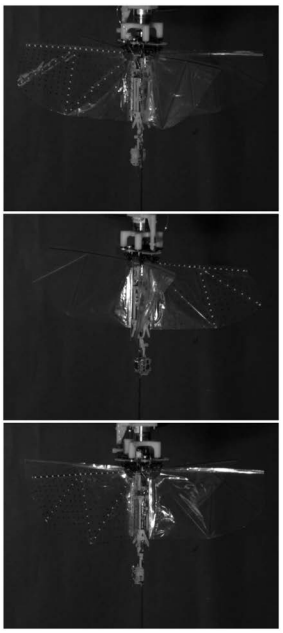

Figure 5: Snapshots of high speed video from three viewing angles.

## 4 Results and Discussion

### 4.1 Pitch Input

Pitch input was tested at $-1.5° \leq \delta_p \leq 1.5°$ with $\delta_r = 0°$. Figure 6 and 7 show the cycle-averaged forces and moments versus the pitch input.

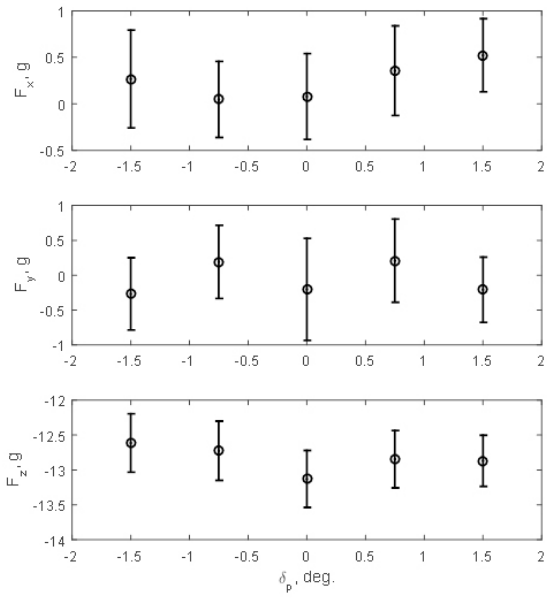


Figure 6: Cycle-averaged forces vs. pitch input.

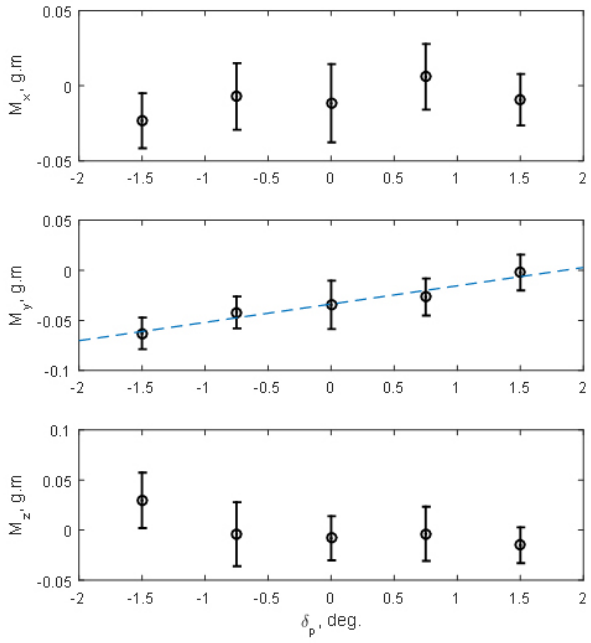


Figure 7: Cycle-averaged moments vs. pitch input.

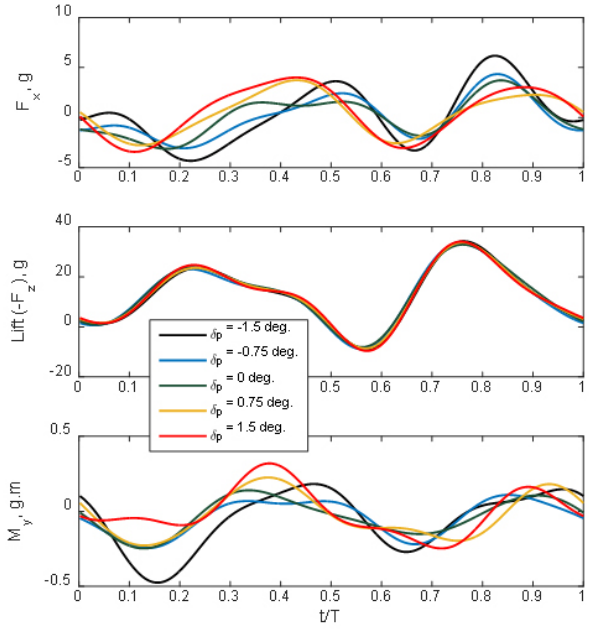


Figure 8: Time-resolved forces and pitching moment for various pitch inputs.

The pitching moment exhibits a linearly increasing trend in the figure. Other force and moment components are less affected by the input. The lift ($-F_z$) shows small decreases when the wings are tilted to either directions, but the drop is within 0.5g. The yawing moment ($M_z$) is also slightly affected nonlinearly, but it is likely due to small unequal tilt of left and right wings because the wings were tilted by different servos, it is very difficult to ensure both sides are tilted at the exact same angle.

The time-resolved forces and pitching moment is shown in Figure 8. The data starts at the beginning of upstroke, upstroke ends at $t/T$ = 0.53, and down stroke ends at $t/T$ = 1, consistent with the identified stroke angle shown in Figure 9. From Figure 8, tilting the wing roots rearward has very little effect on the lift ($-F_z$), but it causes significant increase on the forward force ($F_x$) during upstroke, staring at $t/T$ = 0.15. This is consistent with the larger rotation angle at the 0.55 wingspan shown in Figure 10. Larger rotation angle during upstroke translates to larger angle of attack, thus creating larger drag, which results in larger forward force. Larger forward force should contribute to larger pitch up moment because the centre of force should be located lower than stroke plane, where the CG is assumed to be. The forward force and pitching moment are highly correlated, both are most affected by the wing roots tilting during the upstroke. Pitching moment can be contributed by the forward force and lift dissymmetry between the front and rear wings. It is quite difficult to evaluate the front-rear lift dissymmetry because the load cell measures only the total lift, but the wing kinematics might provide a probable explanation.

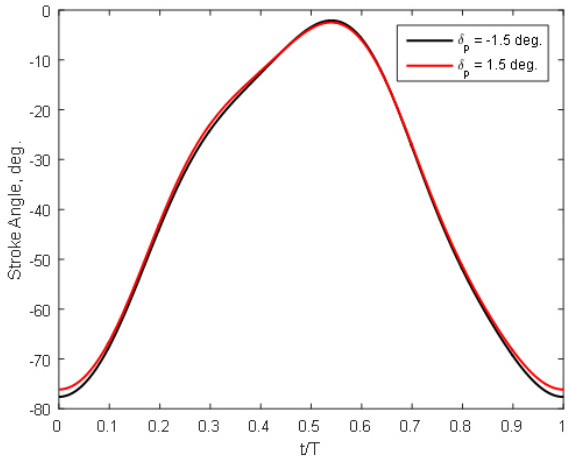


Figure 9: Stroke angle of the pitch input cases.

Figure 11 shows the clap-and-fling between the right and left front wings. Only the cross section of the left front wing is reconstructed, the right front wing is mirrored. Timestamps are shown on the figure so that the wing cross section can be associated correctly with data in Figure 8 to 10. The wings are far apart during the clap-and-fling, which is something that requires further improvement on the flapping mechanism. It

is also due to the distortion caused by data projection in a flat plane.

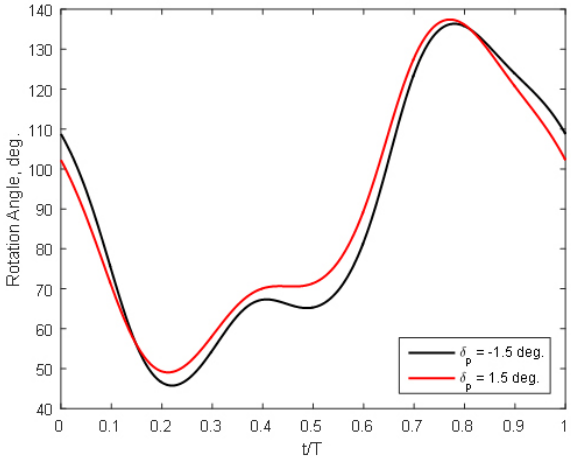


Figure 10: Rotation angle at 0.55 wingspan of the pitch input cases.

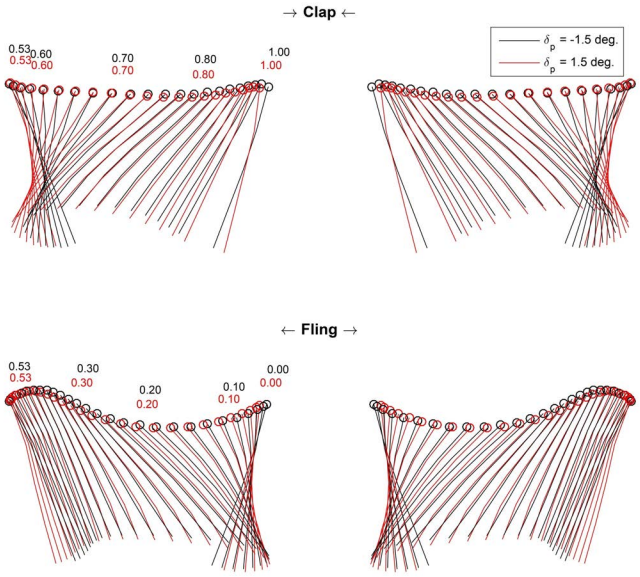


Figure 11: Clap-and-fling at 0.55 wingspan of the pitch input cases.

As seen in Figure 11, as the wings are tilted rearward ($\delta_p = 1.5°$), the wings are under tension when they clap. It causes the wing to have slightly lesser stroke angle and wing rotation occurs earlier. The earlier wing rotation could produce more effective clap-and-fling, which produces higher lift on the front wings compared to the rear wings, and contributes to the higher pitching moment.

In summary, tilting the wing roots to the rear can create a linearly increasing trend in the pitching moment while the other force and moment components are less affected. The increase of pitching moment could be due to increase of drag during upstroke and the lift dissymmetry between front and rear wings caused by more effective clap-and-fling on the front wings.

### *4.2 Roll Input*

Roll input was tested at $-1.5° \leq \delta_r \leq 1.5°$ with $\delta_p = 0°$. Figure 12 and 13 show the cycle-averaged forces and moments versus the roll input. Similar to the pitching case, the rolling moment exhibits a linearly increasing trend in the figure. Other force and moment components are less affected by the input. The lift ($-F_z$) shows small decreases when the wings are tilted to either directions, but the drop is within 0.5g. Unlike the pitching case, the yawing moment ($M_z$) is not affected at all. Different from the pitching arms, the rolling arm is driven by one servo only. Due to the similarity of how the wings are being tilted in both the rolling and pitching cases, the fact that the yawing moment is not affected in the rolling case proves that the effect on yawing moment in the pitching case is caused by unequal tilt of the left and right wings.

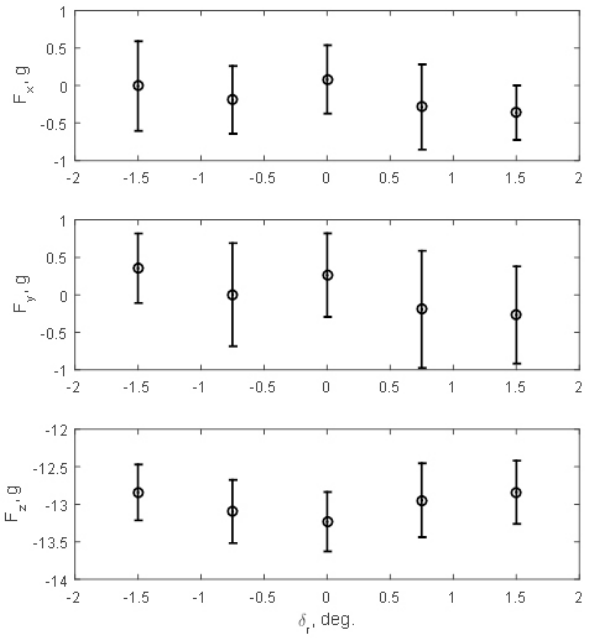


Figure 12: Cycle-averaged forces vs. roll input.

The time-resolved forces and rolling moment is shown in Figure 14. Similar to the pitching case, the data starts at the beginning of upstroke, upstroke ends at $t/T$ = 0.53, and down stroke ends at $t/T$ = 1, consistent with the identified stroke angle shown in Figure 15.

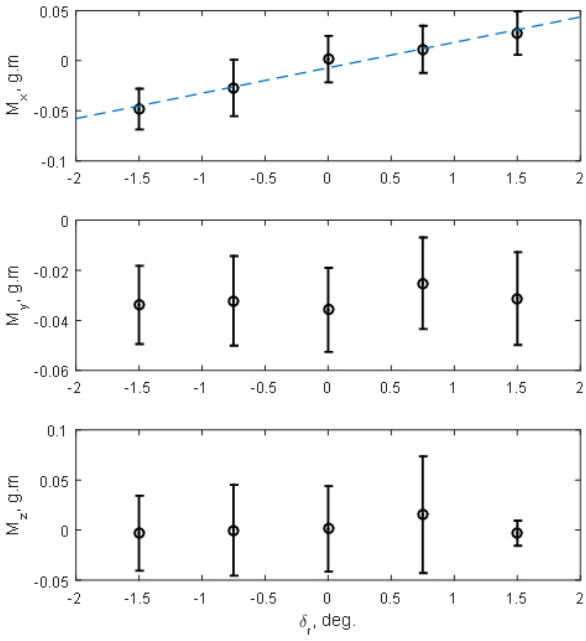


Figure 13: Cycle-averaged moments vs. roll input.

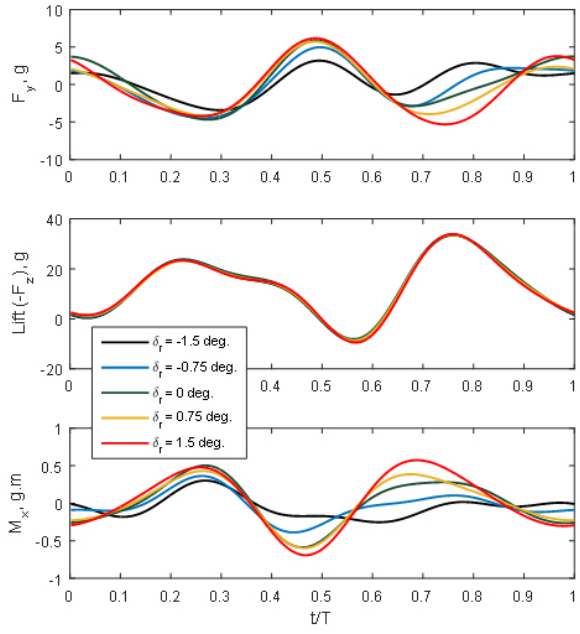


Figure 14: Time-resolved forces and pitching moment for various roll inputs.

From Figure 14, tilting the wing roots rightward has very little effect on the lift ($-F_z$), but it causes significant magnitude increase on the rightward force ($F_y$) during down stroke, staring at t/T = 0.65. This is consistent with the lesser rotation angle at the 0.55 wingspan shown in Figure 16. Lesser rotation angle during down stroke translates to larger angle of attack which results in higher drag. The drag causes larger negative rightward force during down stroke. The negative rightward force contributes to the roll right moment.

The rightward force and the rolling moment are inversely correlated, both are most affected by the wing roots tilting during the down stroke. Rolling moment can be contributed by negative rightward force and lift dissymmetry between the left wings and the right wings.

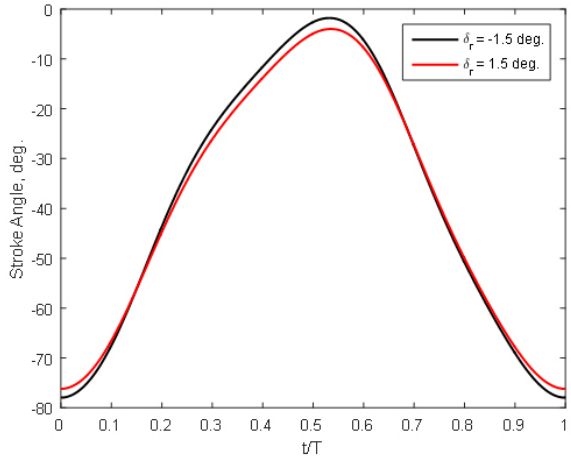


Figure 15: Stroke angle of the roll input cases.

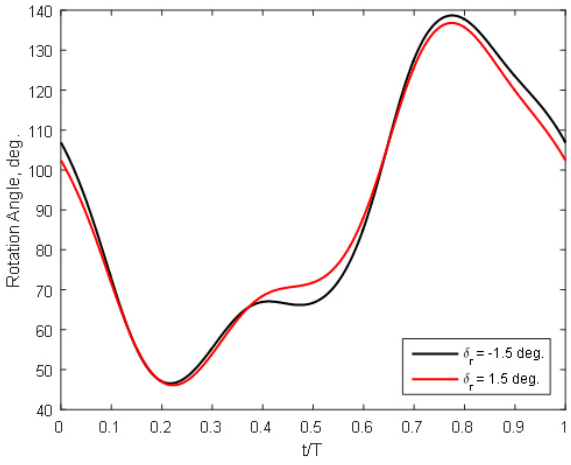


Figure 16: Rotation angle at 0.55 wingspan of the roll input cases.

Figure 17 shows the clap-and-fling between the left front and the left rear wings. Only the cross section of the left front wing is reconstructed, the left rear wing is mirrored.

Timestamps are shown on the figure so that the wing cross section can be associated correctly with data in Figure 14 to 16. Due to reasons mentioned earlier, the wings seem to be further apart than reality.

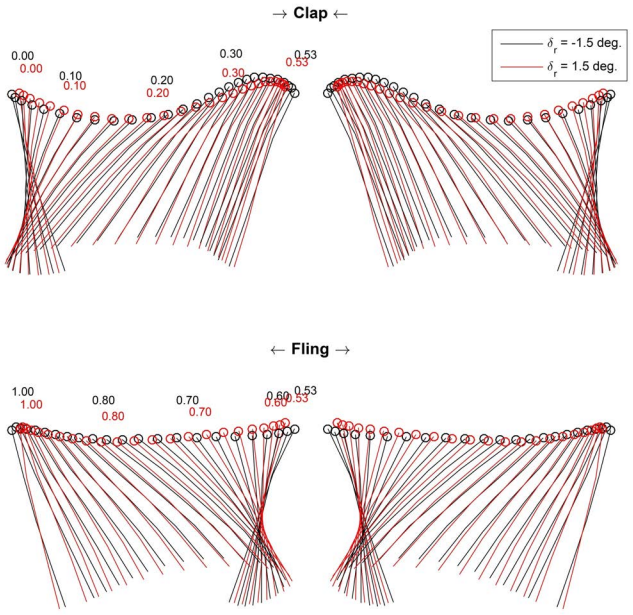


Figure 17: Clap-and-fling at 0.55 wingspan of the roll input cases.

Similar to the pitching case, as the wings are tilted rightward ($\delta_r = 1.5°$), the wings are under tension when they clap. It causes the wing to have slightly lesser stroke angle and wing rotation occurs earlier. The earlier wing rotation could produce more effective clap-and-fling, which produces higher lift on the left wings compared to the right wings, and contributes to the higher rolling moment.

In summary, tilting the wing roots to the right can create a linearly increasing trend in the rolling moment while the other force and moment components are less affected. The increase of rolling moment could be due to larger drag during down stroke and the lift dissymmetry between left and right wings caused by more effective clap-and-fling on the left wings.

### *4.3 Effect of Centre of Gravity Shift*

It is expected that if the CG is shifted far upward or downward, the pitching and rolling moments will be dominated by the effect of forward and rightward forces respectively. Given the fact that the cycle-averaged values of the forces do not exhibit any trend with the tilt angles, it is very likely that the observed linear trend of pitching and rolling moment shown in Figure 7 and 13 would only occur if the CG is within certain range where the effects of lift dissymmetry are dominant.

To evaluate this, the moments were transformed into different coordinate systems. The coordinate systems were shifted up and down from the original position by $\Delta l_z$. Positive $\Delta l_z$ indicates shifting down. the figure of merit in this evaluation are the linear fit slope and the norm of residual of the linear fit. The linear fit slope indicates the effectiveness of the moment generation, the higher the number, the more effective it is. The norm of residual indicates the linearity of the trend, the lower the number, the more linear it is.

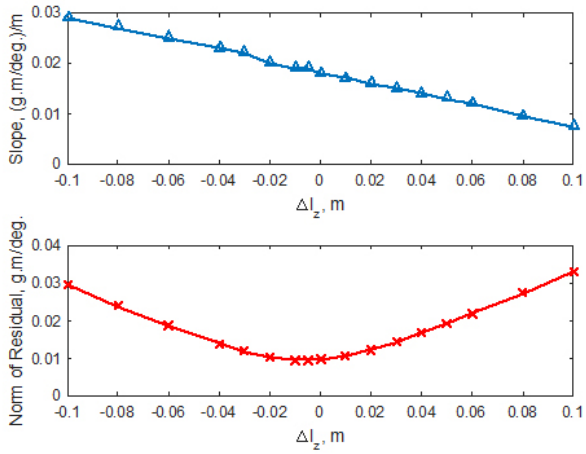


Figure 18: Slope and norm of residual of linear fit of pitching moment vs. pitch input at various CG locations.

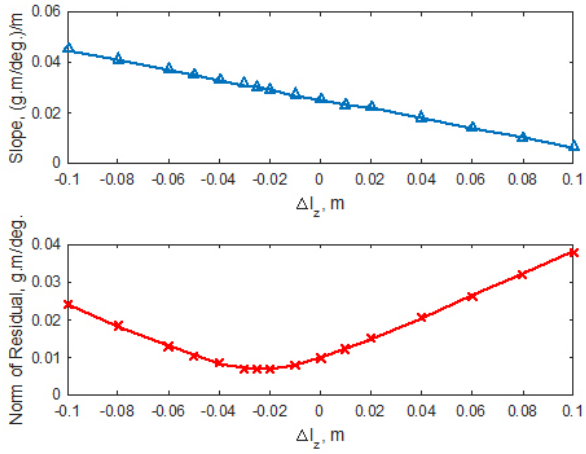


Figure 19: Slope and norm of residual of linear fit of rolling moment vs. roll input at various CG locations.

As shown in Figure 18 and 19, the higher the CG is, the more effective the moment generation is. In other words, having the CG positioned very low would make the wing tilt mechanism useless. Having the CG positioned very high is also not desirable because the trend might become highly nonlinear. The best location of the CG is between 0 to 30mm above the stroke plane as far as linearity is concerned. This

finding is very interesting because the effectiveness and linearity of this tailless control mechanism on similar flapping wing platform has to be taken into account during the design stage of the flying machine.

### *4.4 Roll-Pitch Coupling*

There are two types of couplings between pitch and roll. One is the mechanical coupling which is caused by the design of the mechanism. In this case, the pitching arms are installed on the rolling arm. Rotating the rolling arm would change the pitching arm angle by a little. Another type of coupling is the aerodynamic coupling, which is caused by the aerodynamics effect when the wings are tilted forward-rearward and left-right at the same time.

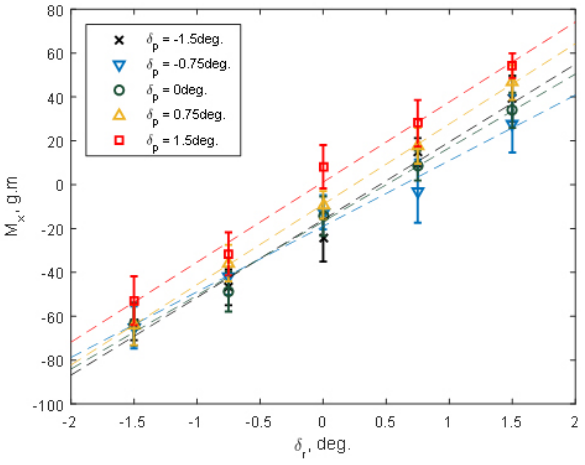


Figure 20: Coupling effect on rolling moment.

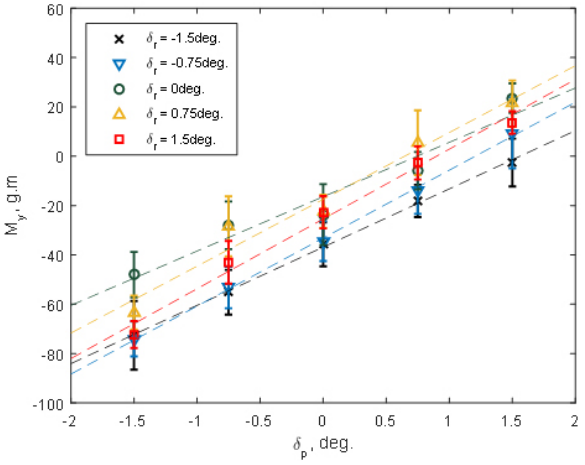


Figure 21: Coupling effect on pitching moment.

The mechanical coupling of this mechanism is very small due to the small tilting angles and the utilization of ball link, but aerodynamic coupling is unavoidable. This paper does not take the effort to explain the coupling, but simply to investigate the significance of the coupling effect.

Figure 20 and 21 show the coupling effect on rolling moment and pitching moment. Generally, the linear relationship retained, but the trim point (zero moment) shifted. The coupling seems to have more significant effect on the trim point than the linearity. While the linear slopes are quite similar, the trim point shifts in an ambiguous pattern.

## 5 Conclusion

A tailless control mechanism was designed, fabricated, and tested on a four-winged double clap-and-fling flapping wing platform. The mechanism tilts the wing roots in forward-rearward and left-right directions creating pitching and rolling moments respectively. Tilting the wings rearward and rightward create positive pitch up and roll right moments respectively. The change in pitching moment is caused by the change in forward force and the front and rear wings lift dissymmetry. But the linear trend is very likely to be cause by the lift dissymmetry because as the CG is shifted far up and far down, where the forward force effect is dominant, the linearity is not retained. Similarly, the linearity of the rolling moment is likely to be caused by the left-right wings lift dissymmetry.

From the wing kinematics, the lift dissymmetry is believed to be cause by the earlier wing rotation at the end of the stroke which resulted in a more effective clap-and-fling. However, this claim has to be further investigated.

The best CG position to maintain linearity of the moments is found to be in between 0 to 30mm above the stroke plane. This is quite a high CG configuration, and very difficult to achieve on flying platform.

Coupling between pitch and roll control are also shown in the paper. Generally, when pitch and roll inputs are applied together, the linearities of the moments are retained, but result in an ambiguous shift of the trim point.

## Acknowledgements

Authors appreciate the financial support from Future System and Technology Directorate of Singapore (Programme No. PA 9014100626).

## References

[1] Q.V. Nguyen, W.L. Chan, and M. Debiasi. Hybrid design and performance tests of a hovering insect-inspired flapping-wing micro aerial vehicle. *Journal of Bionic Engineering*, 13(2):235–248, 2016.

[2] Q.V. Nguyen, W.L. Chan, and M. Debiasi. Performance tests of a hovering flapping wing micro air vehicle with double wing clap-and-fling mechanism. In *International Micro Air Vehicle Conference and Competition (IMAV)*, 2015.

[3] W.L. Chan, Q.V. Nguyen, and M. Debiasi. Pitch and yaw control of tailless flapping wing mavs by implementing wing root angle deflection. In *International Micro Air Vehicle Conference and Competition (IMAV)*, 2014.

[4] W.L. Chan, K.S. Cheng, and Q.V. Nguyen. Investigation on tailless control of a flapping wing mav. In *International Micro Air Vehicle Conference and Competition (IMAV)*, 2015.

[5] M. Karasek, I. Romanescu, and A. Preumont. Pitch moment generation and measurement in a robotic hummingbird. *International Journal of Micro Air Vehicles*, 5(4):299–310, 2014.

[6] M. Karasek, A. Hua, Y. Nan, M. Lalami, and A. Preumont. Pitch and roll control mechanism for a hovering flapping wing mav. In *International Micro Air Vehicle Conference and Competition (IMAV)*, 2014.

[7] M. Takagi, T. Nishimura, and T. Miyoshi. Development of a roll and yaw moment generation mechanism with flapping amplitude control. *Journal of Aero Aqua Biomechanisms*, 4(1):56–62, 2015.

[8] H.V. Phan and H.C. Park. Pitch, roll, and yaw moment generator for insect-like tailless flapping-wing mav. In *Proc. SPIE 9797, Bioinspiration, Biomimetics, and Bioreplication*, 2016.

[9] M. Keennon, K. Klingebiel, H. Won, and A. Andriukov. Development of the nano hummingbird: a tailless flapping wing micro air vehicle. In *50th AIAA Aerospace Sciences Meeting*, 2012.

[10] H. Frontzek, E. Knubben, N. Gaissert, R. Mugrauer, G. Mugrauer, A. Jebens, and K. Jebens. Bionicopter. In *FESTO Report 54814 en 4/2013*, 2013.

[11] H. Frontzek, E. Knubben, R. Mugrauer, G. Mugrauer, A. Jebens, K. Jebens, C. Rabe, and N. Gaiert. emotionbutterflies: Ultralight flying objects with collective behaviour. In *FESTO Report 50058 en 4/2015*, 2015.

[12] R.J. Wood. Design, fabrication, and analysis of a 3 dof, 3cm flapping-wing mav. In *In IEEE/RSJ International Conference on Intelligent Robots and Systems (IROS)*, 2007.

[13] K.Y. Ma, P. Chirarattananon, S.B. Fuller, and R.J. Wood. Controlled flight of a biologically inspired, insect-scale robot. *Science*, 340(6132):603–607, 2013.

[14] T. L. Hedrick. Software techniques for two- and three-dimensional kinematic measurements of biological and biomimetic systems. *Bioinspiration and Biomimetics*, 3(3):034001, 2008.